International Journal of Plasticity 41 (2013) 1–13

Contents lists available at SciVerse ScienceDirect

International Journal of Plasticity

journal homepage: www.elsevier.com/locate/ijplas

Dislocation models of interfacial shearing induced by an approaching lattice glide dislocation

H.J. Chu [a,b], J. Wang [a,*], I.J. Beyerlein [c], E. Pan [d]

[a] Materials Science and Technology Division, Los Alamos National Laboratory, Los Alamos, NM 87545, USA
[b] College of Hydraulic Science and Engineering, Yanzhou University, Yangzhou 225009, China
[c] Theoretical Division, Los Alamos National Laboratory, Los Alamos, NM 87545, USA
[d] Department of Civil Engineering, University of Akron, Akron, OH 44325, USA

ARTICLE INFO

Article history:
Received 20 May 2012
Received in final revised form 11 August 2012
Available online 23 August 2012

Keywords:
A. Dislocations
C. Numerical algorithms
B. Anisotropic material
B. Layered material

ABSTRACT

When a lattice glide dislocation approaches a bi-metal interface with relatively low shear strength, it causes the interface to shear. Interfacial shearing is accommodated by the nucleation and growth of interfacial dislocations, which have an attractive interaction with the incoming dislocation. Thus a critical length scale exists at which the net force on the incoming lattice glide dislocation can transition from being initially repulsive to attractive. In this paper, we develop dislocation-based interface shear models in order to represent this mechanism of interface/dislocation interaction at the continuum scale. Three versions are devised with different degrees of complexity and hence computational cost: the continuous shear model (CSM), simplified-CSM model (SCSM), and single dislocation shear model (SDSM). We simulate the interaction processes with these three models by means of a Green's function method for an anisotropic bimaterial. All three models find that the critical length scale at which the dislocation becomes attracted to the interface increases as the interfacial shear resistance decreases. While the most complex model of the three, the CSM, performs the best, the SCSM and SDSM are more advantageous for implementation into higher-length scale dislocation dynamics models.

Published by Elsevier Ltd.

1. Introduction

In the plastic deformation and fracture of metallic composites, the interactions between lattice dislocations and the bi-metal interfaces play a critical role. Dislocation motion is impeded by the presence of interfaces, and the degree of impediment depends on interface structure (Smith and Hashemi, 2006; Demkowicz et al., 2008). The effect of interface structure can be appreciated by considering the class of atomically flat interfaces with a coherent, semi-coherent, or incoherent structure. For coherent and semi-coherent interfaces, an approaching dislocation encounters internal stresses due to the lattice mismatch strain, which it must overcome to reach the interface. Once at the interface, the dislocation is either transmitted across or absorbed and stored in the interface. In the former case, the transmission stress is related to both coherency stresses and the discontinuity of slip systems across the interfaces (Wang and Misra, 2011; Wang et al., 2012b). Earlier atomistic simulations performed by Hoagland et al. (2002) showed that the peak strength of coherent Cu/Ni multilayers at layer thicknesses below ≈5 nm may be interpreted in terms of the high coherency stresses that must be overcome for the single dislocation transmission. For semi-coherent interfaces, even though the coherency stresses may be partially relaxed, the misfit dislocations provide another obstacle in which the glide dislocation must cut-through (Hoagland et al., 2002). In the event

* Corresponding author. Tel.: +1 505 667 1238.
E-mail address: wangj6@lanl.gov (J. Wang).

0749-6419/$ - see front matter Published by Elsevier Ltd.
http://dx.doi.org/10.1016/j.ijplas.2012.08.005

the lattice glide dislocation is absorbed in coherent or semi-coherent interfaces, theoretical models at both the continuum scale and discrete dislocation dynamics have been developed to describe the dissociation and subsequent spreading of its core (Anderson and Li, 2001; Shen and Anderson, 2006, 2007; Shehadeh et al., 2007).

Unlike coherent and semi-coherent interfaces, within a certain distance from an incoherent interface, a run-in dislocation can be attracted to it. The attraction force results from in-plane shearing of the incoherent interface. Before the dislocation reaches an incoherent interface, its stress state causes the interface to shear via the nucleation and glide of interfacial dislocation loops (Hoagland et al., 2006; Wang et al., 2008a,b). Once created, these interfacial glide loops attract the lattice glide dislocation to the interface. This mechanism was simulated by molecular dynamics simulations (Wang and Misra, 2011; Wang et al., 2012b). The latter studies further showed that the spatial extent of this attraction force on the lattice glide dislocation increases as the interfacial shear strength decreases. The influence of interface structure and properties, like its interfacial shear strength, on dislocation/interface interactions has yet to be incorporated into larger scale models for the deformation behavior of polycrystalline metals. At present, most polycrystal models assume that interfaces, grain boundaries, or twin boundaries lead to Hall–Petch-type hardening, voids, or deformation twins (Barbe et al., 2001; Ohashi, 2005; Brown et al., 2012). Some others consider full or twinning dislocations to penetrate the grain boundaries or interfaces provided that the slip systems across the interface are geometrically well aligned (Ashmawi and Zikry, 2002; Roters et al., 2010; Bieler et al., 2009; Beyerlein et al., 2011). None of these models, however, attempt to account for dislocation/interface interactions in the cases of weak interfaces, wherein the interfacial shear properties matter.

One desirable method for making such a transition from atomic scales to polycrystalline scales is development and implementation of dislocation-based models. A few classes of models have been developed to treat individual, discrete dislocations: discrete dislocation dynamics simulation (Ghoniem and Sun, 1999; Ghoniem et al., 2000; Wang and Ghoniem, 2006; Devincre et al., 2008; Espinosa et al., 2006; Akasheh et al., 2007; Zbib et al., 2011; Erturk et al., 2009; Balint et al., 2008), phase field modeling (Shen and Wang, 2004; Hu et al., 2004; Koslowski et al., 2002; Hunter and Koslowski, 2008; Hunter et al., 2011), and Green's function techniques (Wang, 1996; Ma et al., 2006; Chu et al., 2011, 2012a,b). In many instances, these have proven successful in using atomic-scale results for improved predictions in single and multi-crystal problems (Cao et al., 2010; Hunter et al., 2011; Wang and Beyerlein, 2012; Wang et al., 2012a).

In this article, we utilize a two-dimensional (2D) Green's function technique for bi-metal interfaces (Ting, 1996; Pan and Amadei, 1999) to build dislocation-based models for the interaction of an approaching lattice glide dislocation with an incoherent interface that is weak in shear. Three such models with different levels of sophistication are presented, in order to provide some versatility in the type of polycrystalline model in which they can be implemented. The study focuses on two aspects: (1) the relative level of accuracy of the three models and (2) the critical length scale at which an approaching lattice glide dislocation becomes drawn to the interface and its dependence on interfacial properties. In application, the simulations consider two elastically anisotropic, dissimilar crystals with a common incoherent interface and its interaction with an impinging screw dislocation. Results show that the proposed continuous shear model (CSM), which represents interface shearing by a continuous distribution of interfacial dislocations, is able to quantitatively describe the interaction as reported by atomic-scale simulation. For the purposes of modeling such interface/dislocation interactions in higher length scale models, we introduce two simpler dislocation models, involving a super interfacial dislocation, that are also capable of reasonable quantitative prediction, provided that the Burgers vector of the super dislocation is 'calibrated' to give the correct interaction force. These models find that there is a critical interaction distance at which the screw dislocation will be drawn towards the interface, suggesting an optimal layer thickness (or crystal size) at which we can expect little dislocation storage in the crystals. Further, they show that interfaces weaker in shear produce a stronger attraction force. These results are applicable to the first stage of dislocation/interface interaction, before the lattice glide dislocation touches and reacts with the interface. After it reaches the interface, a dislocation can be absorbed, transmitted, or annihilated, processes that will also depend on the interfacial shear properties of the interface, a subject we leave for future study.

2. Dislocation-based interface shear models

2.1. Interfacial shearing via nucleation of interfacial dislocations

The present models apply to the interaction of a lattice glide dislocation with an atomically flat incoherent interface. Such interfaces represent a broad class of interfaces where the bounding crystals do not have the same lattice parameter and/or do not share the same crystal structure. No coincident-site-lattice (CSL), boundary unit cell (BUC) or periodicity in the interface exists. However, it could be energetically favorable for such an incommensurate interface to take on a pseudo-periodic pattern in the form of extended periodic arrays of BUC-like features (Demkowicz et al., 2008). For a fixed orientation relationship and interface plane, such interfaces can possess many metastable states that differ in energy by relatively small amounts and are separated by small energy barriers. Consequently, in response to a mechanical load, they may easily change from one state to another, which is accomplished by the nucleation and motion of interfacial dislocations, whose Burgers vectors are defined by the BUC of the pseudo-repeatable pattern, but whose magnitude and line orientation can vary widely. Accordingly, there are many possible combinations of sets of Burgers vectors that can accomplish a given interfacial distortion, such as interfacial shearing. (We note that this is not the case for a coherent interface, where the Burgers vector of the interfacial dislocation can be determined based on the coherent dichromatic pattern.) The main requirement is that the net

Burgers vector of the interfacial dislocations induced during loading is equal to that prior to application of the load, which is zero.

2.2. Interfacial shear induced by an approaching lattice glide dislocation

The case of interest here is the change in structure of the interface in response to a run-in glide dislocation from the adjoining crystal. Atomistic simulations show that as a lattice glide dislocation approaches the interface, the interface can readily shear under the stress field of an impinging glide dislocation. Interfacial shearing is accomplished through the creation and growth of dislocation glide loops within the interface, whose Burgers vector lies in the plane of the interface (Demkowicz et al., 2008; Wang et al., 2008a,b). The critical stress for the nucleation of these loops corresponds to what we will refer to as the interface shear strength (ISS). The interaction between the glide loops and the run-in lattice glide dislocation is attractive, causing the dislocations to be drawn to the interface (Hoagland et al., 2006; Wang et al., 2012b).

Fig. 1 presents a schematic of this dislocation/interface interaction. Fig. 1a shows the elastic shear stress field along the interface produced by the incoming glide dislocation. The field has two peaks, which increase in magnitude and width as the lattice screw dislocation approaches the boundary. When the shear stress exceeds the ISS, interfacial dislocation loops will nucleate in these peak regions, each is indicated by a dislocation dipole in Fig. 1b. With the introduction of these dipoles, the peak shear stress becomes equal to or less than the ISS (Fig. 1c) as a result of the superposition of stresses in Fig. 1a and b. The amount of shear displacement contributed by each dislocation loop is limited by its Burgers vector b_l. Accordingly, as the load increases further, the peak shear will eventually rise again to exceed the ISS. When this happens, a second set of dislocation dipoles, one for each peak, must nucleate at the peak locations. As the interaction progresses, we can expect that as the lattice glide dislocation approaches the interface and the applied shear on the interface increases, the number of interfacial dislocations increases and the sheared region over which they are distributed broadens. Eventually, when the lattice glide dislocation reaches the interface, it reacts with these interfacial dislocations.

To accomplish the shear that develops over a broad interfacial shear zone, a distribution of interfacial dislocation loops is required. As discussed above, due to the energetic landscape of these incoherent interfaces, the interfacial shear displacements could be achieved through an infinite number of possible distributions of interfacial dislocations. The challenge we

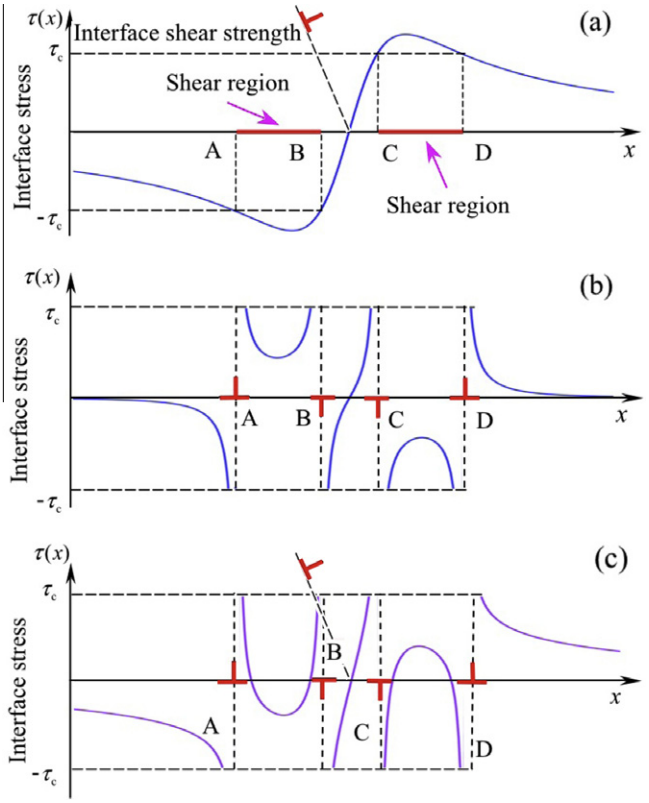

Fig. 1. Illustration of the mechanism of interfacial shearing induced by a nearby screw dislocation. The interfacial shear strength is denoted by τ_c: (a) Distribution of shear stress distribution along the interface plane due to an approaching screw dislocation. Note that the shear stress in regions AB and CD exceeds the interface shear strength. (b) Distribution of shear stress on the interface due to two pairs of interfacial dislocation dipoles introduced in regions AB and CD. (c) Total shear stress distribution along the interface due to both the screw and interfacial dislocations.

address in this work is developing a dislocation based model for the nucleation and distribution of these interfacial glide loops as a function of interfacial shear properties that captures the dislocation/interface interaction kinetics observed in atomic-scale simulation.

2.3. Dislocation-based interface shear models

To begin, we assume that nucleation of interfacial glide dislocations is governed by a maximum shear criterion, $|\tau(x)| \leqslant \tau_c$, where $\tau(x)$ is the total shear stress due to all dislocations in the system along the interface coordinate x and τ_c is the interface shear strength. Before nucleation of an interface dislocations, $\tau(x) = \tau(x{:}\ b_L, m, d)$ meaning that the shear stress profile only depends on that induced by the incoming lattice dislocation, where b_L is the Burgers vector of the incoming lattice glide dislocation, m is the normal of its glide plane, and d is the distance between the lattice glide dislocation and the interface. After nucleation of N interfacial dislocations, the interfacial shear stress field is altered due to the presence of $N+1$ dislocations in the system, and thus becomes also a function of b_I^i ($i = 1,\ldots,N$), the Burgers vector of the N interfacial dislocations, and their positions x_i in the interface. Therefore we can generalize the maximum shear criterion to $|\tau(x)| = |x{:}b_L, m, d;\ b_I^i, x_i, i = 1,\ldots,N)| \leqslant \tau_c$. Under the assumption of linear elasticity, we can apply linear elastic superposition, as a first order approximation, and add the elastic stress fields of all dislocations in the system, which gives:

$$|\tau(x)| = \left| \tau_L(x : b_L, m, d) + \sum_{i=1}^{N} \tau_I^i(x : b_I^i, x_i) \right| \leqslant \tau_c \tag{1}$$

where τ_L ($x{:}b_L,m,d$) is the distribution of the shear stress along the interface in association with the incoming lattice glide dislocation, and $\tau_I^i(x : b_I^i, x_i)$ the shear stress along the interface in association with the ith interfacial dislocation. In this work, the interfacial shear stress field generated as a result of given configuration of lattice and interface dislocations will be calculated by a 2D linear elastic Green's function technique, as will be explained later.

Criterion (1) assumes that N, x_i and b_I^i, for all $i = 1,\ldots,N$ dislocations are known. Let's consider first x_i, the equilibrium position of the ith interfacial dislocation, under the condition that all other variables are known. The locations of each interfacial dislocation can be determined by solving for a set of N equations, each one corresponding to the sum of forces on each interfacial dislocation.

$$\left| F_L^i + \sum_{j=1(j\neq i)}^{N} F_j^i + \Delta\gamma_i \right| \leqslant \tau_P^i b_L^i,\ \ i,j = 1,\ldots,N \tag{2}$$

where F_L^i is the projection of the Peach–Koehler (P–K) force on the interface plane due to the incoming lattice glide dislocation, and F_j^i is the projection of the P–K force on the interface plane due to the interaction with the jth interfacial dislocation. A positive P–K force is directed in the positive x-direction. $\Delta\gamma_i = \gamma_i^R - \gamma_i^L$ denotes the change in the formation energy of the interface due to the glide of the ith interface dislocation where γ_i^R and γ_i^L are the formation energies of interfaces to the right and left of the ith interfacial dislocation. Unless stated otherwise, we assume that $\Delta\gamma_i$ is zero, or equivalently, the interfacial Burgers vectors generated accommodate the shear strain by reconfiguring the interface from one metastable state to another, as shown in Fig. 2. The Peierls stress τ_P^i associated with the ith interfacial dislocation b_I^i within the interface is assumed to be proportional to the ISS, i.e., $\tau_P^i = \alpha\tau_c$, where the constant α depends on the properties of the interface.

The remaining important issue is the determination of b_I^i and N used to accommodate a given interfacial shear displacement. For this, we propose three dislocation-based interface shear models: the continuous shear model (CSM), a simplified version of the continuous shear model (SCSM), and a single dislocation shear model (SDSM). The physical difference between them is illustrated in Fig. 3. Each is discussed in the following sections.

2.3.1. Continuous shear model (CSM)

The first dislocation-based model for interfacial shearing is the continuous shear model (CSM). As the lattice glide dislocation approaches the interface, interfacial dislocations will nucleate continuously at the peak regions where the shear stress on the interface plane exceeds the interface shear strength (Fig. 3a). After each is created, they glide away from the nucleation site in order to accommodate the shear strain. This process repeats, creating a continuous distribution of interfacial dislocations in the interface, which can be described as a double-ended pileup (Fig. 3a). Assuming they all have the same Burgers vector, the positions of these dislocations in the sheared region $-l/2 \leqslant x \leqslant l/2$ are described as (Hirth and Lothe, 1992)

$$n_I(x) = \frac{1}{b_I}\frac{db_I}{dx} = \frac{2(1-\nu)\tau}{\mu b_I}\frac{2x}{l^2 - 4x^2} \tag{3}$$

where $n_I(x)$ denotes the dislocation density, b_I is the magnitude of the Burgers vector of the interfacial dislocation, and μ and ν are the shear modulus and Poisson's ratio, τ is the stress applied on the dislocation pileup. Thus, one of the first dislocation dipole is located at the left end, x_1^L, and the other is located at the right end, x_1^R. The dislocations in association with the ith dislocation dipole are denoted as x_i^R and x_i^L. As all interfacial dislocations have the same b_I, the total Burgers vector in association with the sheared region is mb_I where m is the number of the dislocation dipoles.

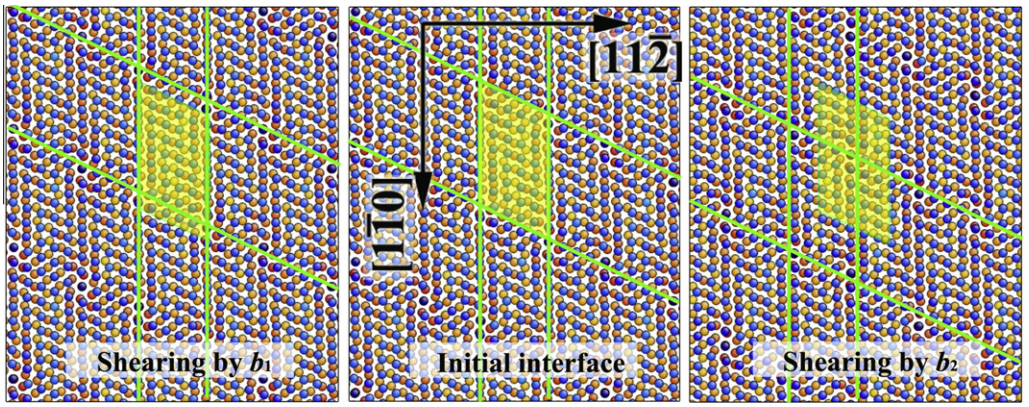

Fig. 2. Atomic structures of the interface after shearing in different directions. The initial interface before shearing is shown in the middle; the interface under shearing by an interfacial dislocation with Burgers vector $\boldsymbol{b}_1 = 1/2\ [\bar{1}\,1\,0]$ is shown on the left-hand side; and the interface after shearing by an interfacial dislocation with Burgers vector $\boldsymbol{b}_2 = 1/4\ [\bar{1}\,1\,0]$ is shown on the right-hand side. The green lines indicate the pseudo-repeatable pattern in each interface, and the yellow shadow represents the unit cell. In order to show the shift of the pattern due to shearing, the yellow shadow is placed in the same position as in the initial interface. Thus, for the interface on the left-hand side, the pattern is simply shifted along the direction of the Burgers vector $\boldsymbol{b}_1$, whilst for the interface on the right-hand side, it is shifted along the direction of the Burgers vector $\boldsymbol{b}_2$. (For interpretation of the references to color in this figure legend, the reader is referred to the web version of this article.)

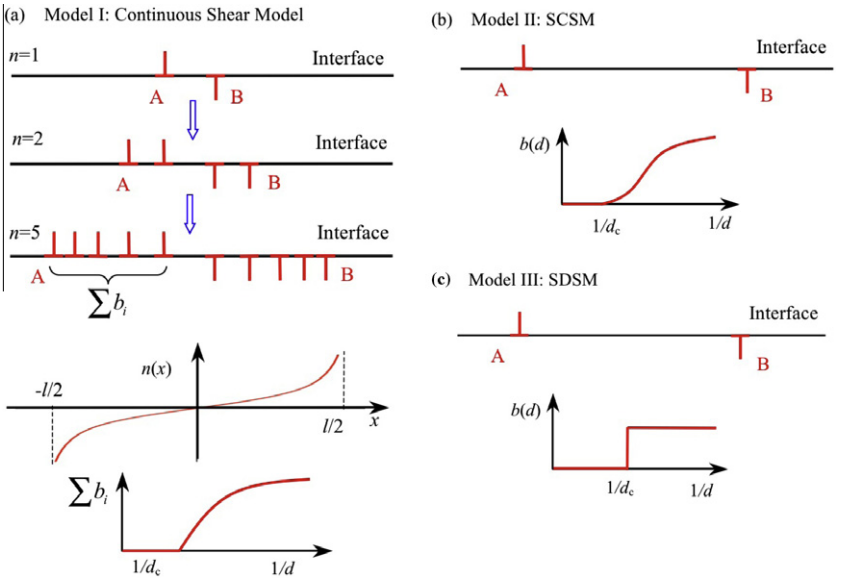

Fig. 3. Conceptual descriptions of three dislocation-based interface shear models: (a) Model I: the continuous shear model (CSM), continuous nucleation of interfacial dislocation loops starting from one dislocation dipole to multiple dipoles as the lattice dislocation approaches the interface. The interfacial dislocation distribution in the sheared region can be described as a stressed double-ended pile-up. (b) Model II: simplified continuous shear model (SCSM), in which continuous nucleation of interfacial dislocations is modeled instead by a single dipole whose Burgers vector increases with decreasing distance between the lattice glide dislocation and the interface. (c) Mode III: single dislocation shear model (SDSM), in which the interface shear is achieved through the nucleation and glide of a single dislocation dipole whose Burgers vector is constant.

We employ the following iterative procedure for a given b_1 to determine the corresponding number of interfacial dislocations n, the location of the two ends x_1^L, and x_1^R of the sheared region via Eq. (2), and the positions of all dislocations in-between using Eq. (3). The algorithm begins with the lattice glide dislocation located in the crystal a sufficient distance d_0 away from the interface such that the shear stress distribution $\tau(x)$ it produces on the interface just exceeds the interfacial shear strength. From this initial $\tau(x)$, we locate the regions of peak shear, I (AB) and II (CD), as illustrated in Fig. 1a. For all configurations, the resulting $\tau(x)$ distribution is calculated by a method based on linear elastic dislocation theory, which in our case will be a Green's function technique.

(a) For distance d_0, the number of interfacial dislocations is initially set to one, i.e., $n = 1$. The single dipole has its ends initially located at the boundaries where the shear stress exceeds the interface shear strength.

(b) Using Eq. (2), we calculate $x_1^{\mathrm{L}}(d_0)$ and $x_n^{\mathrm{R}}(d_0)$ for this dipole. We then compute the shear stress $\tau(x = x_{\mathrm{m}}, n = 1, d_0)$ at the center of the sheared region, given by $x_{\mathrm{m}} = \frac{1}{2}(x_1^L + x_1^R)$.

(c) If $\tau(x = x_{\mathrm{m}}, n = 1, d_0)$ satisfies Eq. (1), we obtain the three variables n, $x_1^{\mathrm{L}}(d_0)$ and $x_1^{\mathrm{R}}(d_0)$ for distance d_0. We then move to step (e).

(d) If it does not satisfy Eq. (1), we set $n = 2$, and return to Eq. (2) to solve for the positions $x_1^{\mathrm{L}}(d_0)$ and $x_1^{\mathrm{R}}(d_0)$. The positions of the 2nd pair of dislocations $x_2^{\mathrm{L}}(d_0)$ and $x_2^{\mathrm{R}}(d_0)$, in contrast, are calculated using the stressed double-ended dislocation pileup model in Eq. (3). Then we compute the shear stress at the center of the sheared region. If the shear stress satisfies Eq. (1), we then carry out the next step (e); otherwise, we repeat this step (d), by incrementing the number of interfacial dislocations by one until Eqs. (1) and (2) are satisfied.

(e) The incoming dislocation is advanced closer to the interface, $d_1 = d_0 + \Delta d$. We solve for the positions of the two dislocations $x_1^{\mathrm{L}}(d_1)$ and $x_1^{\mathrm{R}}(d_1)$ using Eq. (2) and then recalculate the shear stress along the interface $\tau(x = x_{\mathrm{m}}, n = 1, d_1)$. If it satisfies Eq. (1), then we draw the lattice dislocation closer to the interface, $d_2 = d_1 + \Delta d$. If Eq. (1) is not satisfied, we then revisit step (d). In all simulations, Δd is optimized to be 0.125 nm to ensure the convergence.

2.3.2. Simplified CSM model (SCSM)

To simplify the CSM model, one can consider that the interfacial dislocation distribution can be approximated by two 'super interfacial' dislocations, one located at each end of the sheared region. These two super dislocations will have Burgers vectors that increase in magnitude with decreasing distance d, as shown in Fig. 3b. Its value as well as the extent of the sheared region can be solved following the same procedure as described for the CSM model. The advantage of SCSM is that we only consider two dislocations while the concept of the CSM is kept.

2.3.3. Single dislocation shear model (SDSM)

It is possible to simplify the CSM and SCSM further by considering a single interfacial dislocation with a constant Burgers vector (see Fig. 3c). The challenge here is that its Burgers vector has to be selected such that within the sheared regions, the shear stress does not exceed the interfacial shear strength.

3. Application to an fcc/bcc Kurdjumov–Sachs interface

A simple system, amenable to mechanistic interpretation, is the well-studied fcc/bcc interface that adopts the Kurdjumov–Sachs (KS) orientation relationship, a low energy interface that is often generated in epitaxial growth (Misra et al., 1998). This interface has a low shear resistance that can easily be sheared under the stress field of a nearby lattice dislocation (Wang et al., 2011a; Liu et al., 2010). For a given binary system, the shear resistance varies depending on the in-plane shear direction (Demkowicz et al., 2008). For Cu/Nb, for instance, it can range from 0.3 to 0.55 GPa (Wang et al., 2008a, 2012b). Here, we will systematically vary the shear resistance from 0.3 to 0.5 MPa.

The bicrystal model of Cu and Nb with a single KS Cu/Nb interface is illustrated in Fig. 4. Following the KS orientation relationship, the x-axis is parallel to $[1\,1\,\bar{2}]_{\mathrm{Cu}}$ and $[1\,\bar{1}\,2]_{\mathrm{Nb}}$, the z-axis parallel to $[1\,\bar{1}\,0]_{\mathrm{Cu}}$ and $[\bar{1}\,1\,1]_{\mathrm{Nb}}$ and the y-axis is perpendicular to the interface plane and parallel to $[1\,1\,1]_{\mathrm{Cu}}$ and $[1\,1\,0]_{\mathrm{Nb}}$. The incoming lattice dislocation is a screw dislocation in Cu that glides on the $(1\,1\,\bar{1})$ plane with Burgers vector $\frac{1}{2}\langle 110\rangle$. Material moduli are $C_{11} = 168.4$ GPa, $C_{12} = 121.4$ GPa and $C_{44} = 75.4$ GPa for Cu, and $C_{11} = 246.0$ GPa, $C_{12} = 134$ GPa and $C_{44} = 28.7$ GPa for Nb (Hirth and Lothe, 1992).

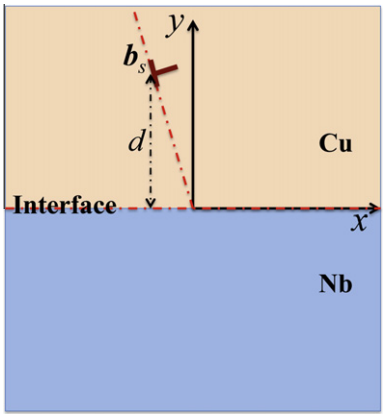

Fig. 4. Corresponding to the KS orientation relationship, the x-axis is parallel to $[1\,1\,\bar{2}]_{\mathrm{Cu}}$ and $[1\,\bar{1}\,2]_{\mathrm{Nb}}$, the z-axis parallel to $[1\,\bar{1}\,0]_{\mathrm{Cu}}$ and $[\bar{1}\,1\,1]_{\mathrm{Nb}}$, and the y-axis is perpendicular to the interface plane and parallel to $[1\,1\,1]_{\mathrm{Cu}}$ and $[1\,1\,0]_{\mathrm{Nb}}$. The incoming lattice glide dislocation is a screw dislocation in Cu that glides on the $(1\,1\,\bar{1})$ plane with Burgers vector $\frac{1}{2}\langle 110\rangle$. The interface plane is on the x–z plane, and d is the distance from the screw dislocation to the interface.

The stress field resulting from the screw dislocation in the crystal, the interfacial dislocations, the interaction between them, and the image force arising from the elastic mismatch across the interface (Koehler force) are calculated using a Green's function method for dislocations in anisotropic bimaterials. Here, we adopt the 2D Green's function method based on complex function theory (Ting, 1996; Pan and Amadei, 1999).

3.1. Influence of elastic anisotropy on interfacial shearing

In the calculations that follow, we choose to use the anisotropic version of the Green's function technique, in spite of the higher computational costs. In calculating the stress field produced on the interface by a run-in dislocation, accounting for the elastic anisotropy of each crystal and the disparity in their elastic anisotropy across the interface is expected to be more accurate than the isotropic approximation. Most metallic crystals are inherently anisotropic, a property that can be indicated by an anisotropic ratio that deviates from the isotropic value of 1. Both crystals considered in the present calculation are well-known to be elastically anisotropic; the anisotropy ratio is 3.2 for Cu and 0.51 for Nb. Before we move onward, we demonstrate a few important differences in the stresses produced between a screw dislocation and Cu/Nb KS interface for the anisotropic and isotropic cases. The effective isotropic shear modulus and Poisson's ratio for Cu are 54.6 GPa and 0.34, and for Nb they are 39.6 GPa and 0.40 (Hirth and Lothe, 1992).

Fig. 5a compares isotropic and anisotropic calculation for the variation of the normalized P–K force acting on the screw dislocation with distance d from an un-sheared interface. As expected, the force follows $F \propto 1/d$. However, the sign of the image force is negative (indicating an attraction) in the isotropic case but positive (a repulsion) in the anisotropic one. The isotropic approximation provides in this case a physically incorrect answer. It is worth mentioning that the self energy of a dislocation is dependent on its characters, such as screw, mixed, or edge type. According to Eqs. (13-148) and (13-156) in the book (Hirth and Lothe,1992) which describes the self energy of a dislocation in an anisotropy media, the energy coefficient k_s for a screw dislocation in anisotropic media is k_s = 42.1 GPa for Cu and 44.3 GPa for Nb, implying that the PK force acting on a screw dislocation in Cu should be repulsive. Which is different from the prediction according to the isotropic solution. However, the PK force acting on an edge dislocation in Cu is attractive, which is consistent with the isotropic solution. In addition, an MD simulation (Wang et al., 2008b) also showed that the pre-factor of the energy of a screw dislocation in Cu crystal (1.547 eV/nm) is lower than that in Nb crystal (1.799 eV/nm), indicating again that the image force on Cu should be repulsive (i.e., positive). Which is consistent with the theoretical solution developed by Barnett and Lothe (1974). Fig. 5b further compares the isotropic and anisotropic predictions for the distribution of shear stresses along the interface plane. Both curves are similar except for a slight difference in their maximum values and a shift in the center of symmetry center. For the isotropic case, the symmetry center is at the origin while it is located at $x \approx 4.8$ nm for the anisotropic case. In summary, due to the accuracy of the anisotropic calculation, all numerical calculations hereinafter are performed using a Green's function method for an anisotropic bimaterial.

3.2. Dislocation–interface interaction in the CSM

3.2.1. Dependence of CSM model on the magnitude of interface dislocation

With the CSM model, we first investigate the effect of the choice of b_I on dislocation/interface interaction. In a given calculation we consider that all the interfacial dislocations have the same Burgers vectors b_I, and between calculations, vary its magnitude in the range of 0.025–0.1 b_s, where b_s denotes the Burgers vector of the approaching screw dislocation. Fig. 6a shows the variation of the PK force on the approaching screw dislocation with its distance d from the interface with the interface shear strength and Peierls stress equal to 0.3 GPa. The CSM captures the transition from initial repulsion by the image force to a net attraction after interfacial dislocations have been nucleated as seen in atomic-scale simulations for the KS interface (Wang et al., 2008b). Fig. 6b and c show respectively that CSM predicts that as the screw dislocation draws closer to the interface, the number of interfacial dislocations and the sheared interfacial region grows. In all cases, reducing b_I does not significantly alter the results, but provides more continuous variations with d.

3.2.2. Interaction dependence on interface properties in the CSM

In this section we study the influence of interface properties on the dislocation-interface interactions. In all cases, $b_I = 0.05 b_s$. Fig. 7b shows the increase in net interfacial dislocation content as the screw glides towards the interface (decreasing d). CSM predicts that as the interfacial shear strength weakens, interfacial dislocations nucleate earlier, when the screw dislocation is further away. Consequently, the critical distance d corresponding to the onset of interfacial dislocation nucleation is higher, 2.90 nm, for τ_c = 0.3 GPa, compared to 2.2 nm for τ_c = 0.4 GPa, and 1.75 nm for τ_c = 0.5 GPa. After interfacial dislocations are created, the net PK force on the dislocation eventually becomes attractive. This is confirmed in Fig. 7a, which compares the variation of the PK force on the approaching screw dislocation with d for different τ_c. As shown, the critical distance corresponding to the net attraction force is higher, 2.6 nm, for τ_c = 0.3 GPa, than 1.9 nm for τ_c = 0.4 GPa, and 1.61 nm for τ_c = 0.5 GPa. As shown in Fig. 7c, a weaker interfacial shear strength produces a larger sheared region for a given d, which, as given in Fig. 7a, corresponds to more interfacial dislocation content. Thus, it can be expected that with more interfacial dislocations, the attraction force on the lattice dislocation at a given distance will be stronger. For example, when the lattice dislocation is 1.5 nm away from the interface, the attraction force acting on the screw dislocation is higher

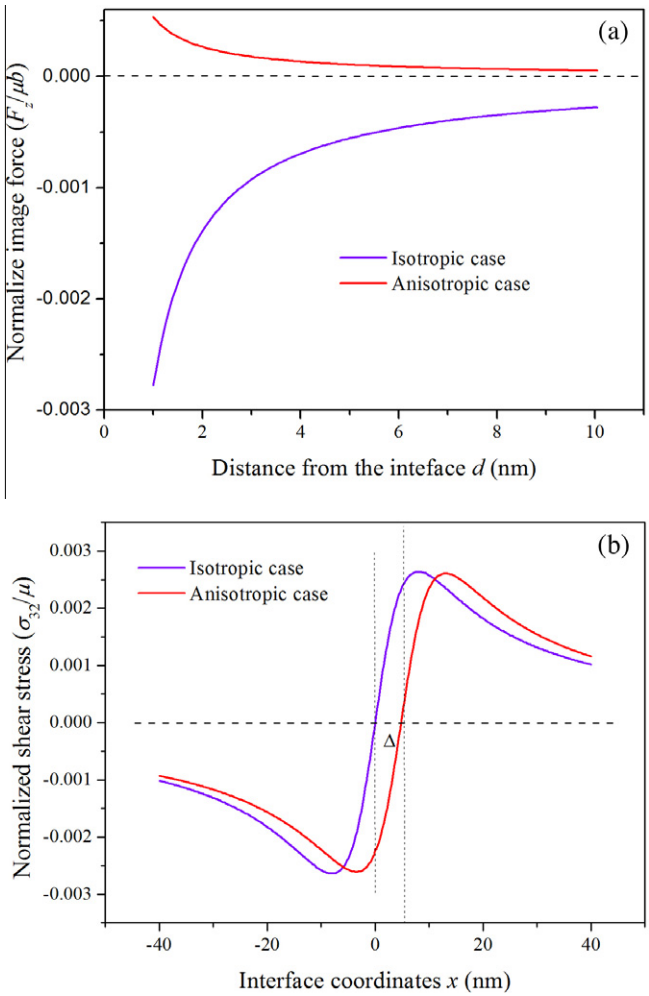

Fig. 5. Comparison between predictions of the Green's function method using the isotropic approximation and full anisotropic properties. (a) The variation of the image force or Koehler force acting on the screw dislocation as a function of the distance from the dislocation to the interface, and (b) the distribution of the shear stresses on the interface plane for both the anisotropic and isotropic cases. (For interpretation of the references to color in this figure legend, the reader is referred to the web version of this article.)

$2.1\mu b$ for $\tau_c = 0.3$ GPa than $1.1\mu b$ for $\tau_c = 0.4$ GPa, and $0.3\mu b$ for $\tau_c = 0.5$ GPa. In summary, weaker interfaces more strongly attract lattice dislocations, which is consistent with MD results (Wang et al., 2011c).

For the calculations in Fig. 7a–c, the Peierls stress equals the interfacial shear strength and the contribution of any changes in formation energy of the interface due to interfacial shearing was neglected. According to Eqs. (1) and (2), altering either will affect the spacing between individual interfacial dislocations and the total extent of the shear region. In this regard, we investigate in Fig. 7d the variation of interface shear region with d for different Peierls stress acting on the interfacial dislocation within the interface. We simply introduce a factor α, which could be greater or less than 1.0, to describe the magnitude, as $\tau_p = \alpha\tau_c$. As shown, a smaller Peierls force leads to a more extended shear region for a given d. The reason is that a greater Peierls force can sustain shorter separation distance between two adjacent interfacial dislocations: 0.5 nm for $\alpha = 2$ and 6.0 nm for $\alpha = 0.8$.

3.3. Interactions in the SCSM and SDSM

We have shown that the CSM captures well the kinetics involved in the interaction between the incoming dislocation and a bi-metal interface. Results from the dislocation based CSM simulations show that interfacial shearing is enabled by the formation of a continuous distribution of interfacial dislocations, each with Burgers vectors much smaller compared to that of the lattice dislocation. Despite its accuracy, directly implementing CSM into a materials code can potentially become too complicated and/or time-consuming. For these reasons, we propose the simplified-CSM and the single-dislocation-shear

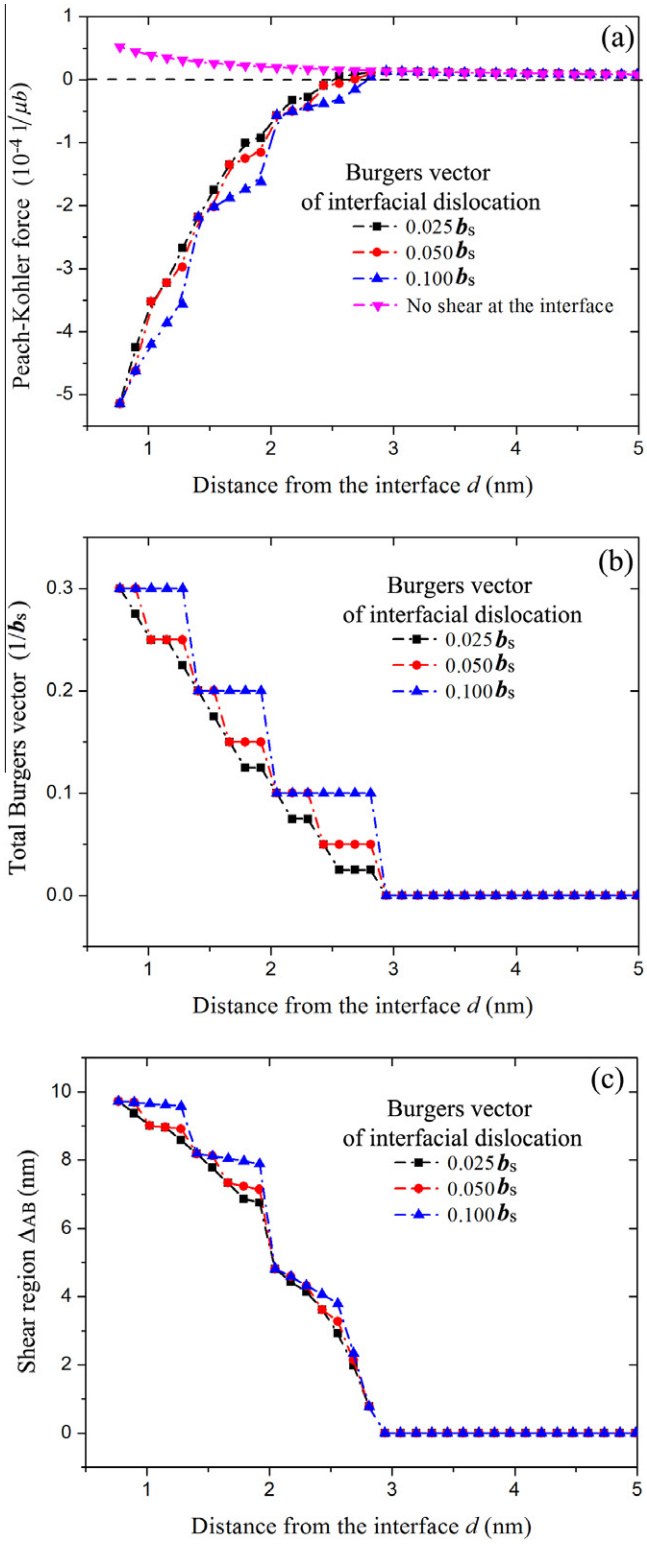

Fig. 6. Simulation of the dislocation–interface interaction by using the CSM: (a) variation of the PK force with d for different Burgers vector of the interfacial dislocation; (b) corresponding variation of the total Burgers vector with d; (c) corresponding variation of the sheared region with d.

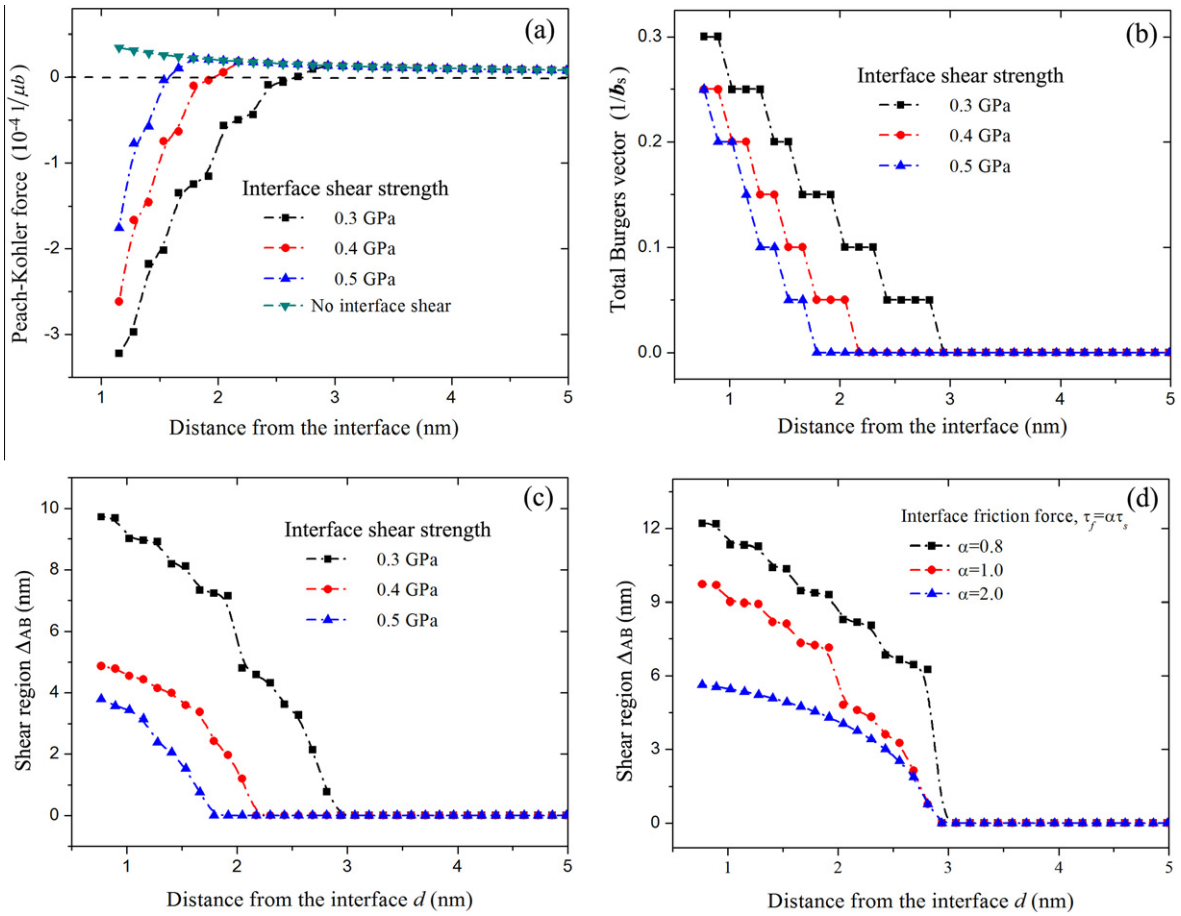

Fig. 7. Influence of the interface properties on the dislocation-interface interaction by using the CSM model: (a) variation of the P–K force with distance for different interface shear strengths; (b) variation of the total Burgers' vector with distance for different interface shear strengths; (c) variation of the sheared region with distance for different interface shear strengths; and (d) variation of the interface shear region with distance for different friction forces.

model (SDSM) as illustrated in Fig. 3b and c, respectively. In this section, we compare the results from these two models with those of CSM.

Fig. 8 compares results from the three models. For this comparison, in the CSM, the increasing interfacial shear is accommodated by increasing the number of interfacial dislocation loops, each with a fixed Burgers vector of value $0.05\boldsymbol{b}_s$, where $\boldsymbol{b}_s$ is the Burgers vector of the lattice dislocation. In contrast, in the SCSM, the number of loops is fixed at one and an increasing interfacial shear is accommodated by increasing the value of its Burgers vector in increments of either $0.025\boldsymbol{b}_s$ or $0.001\boldsymbol{b}_s$. The position of this super interface dislocation is located at the ends of the sheared region and therefore is updated as the extent of the shear region increases. In the SDSM, the interface shear model is further simplified by considering a constant Burgers vector, either $0.30\boldsymbol{b}_s$, $0.17\boldsymbol{b}_s$ or $0.08\boldsymbol{b}_s$.

In comparing the total Burgers vector content in the interface between the CSM and SCSM, three conclusions can be reached: (1) the distance d of the incoming dislocation at which interface dislocations nucleate is the same, (2) the total Burgers vector content is insensitive to the increment in the value of the Burgers vector used in the SCSM, and (3) the magnitude of the total Burgers vector content is larger in the CSM than that in the SCSM (Fig. 8a).

For the SDSM, we find that the constant Burgers vector used for the super interface dislocation in the SCSM can be optimized to give reasonable results. As shown in Fig. 8b, SDSM provides results close to that of CSM when the constant Burgers vector is set to $0.08\boldsymbol{b}_s$. One could also consider optimizing it further by setting it to equal to the total Burgers vector predicted by either the CSM or SCSM. For the same conditions, the CSM provides an approximate upper bound on the Burgers vector content needed, and so the solution obtained via the SCSM reported in Fig. 8a and b is better. Finding the optimal Burgers vector is related to ensuring that the interaction force between the incoming screw dislocation and the interfacial super dislocation, given by $F_{P-K}=\sum_{i=1}^{n} b_s b_i^i f(x_i,d)$. In the CSM, the interaction force between the interfacial and lattice dislocations depends on the distribution of interfacial dislocations and the sheared region. But in the SCSM and SDSM models, the sheared region and the net Burgers vectors determine this force. Since, for the same net Burgers vector content, the sheared region is the largest in the CSM model than the other models, the interaction force is the smallest in the CSM model. Thus in the SDSM

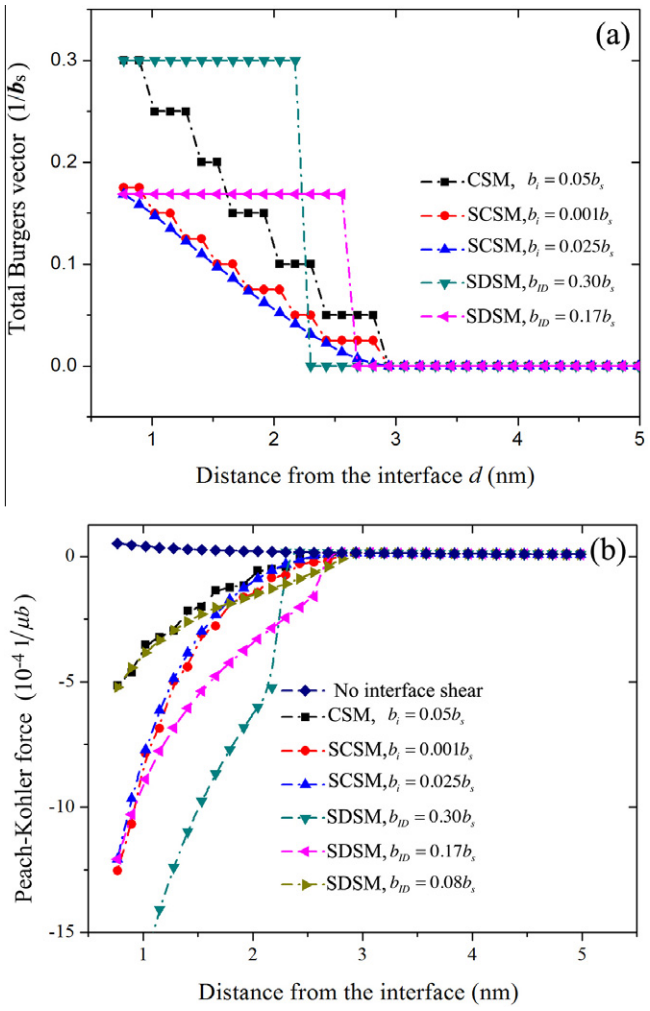

Fig. 8. Comparison of simulation results from the three models: (a) variation of the total Burgers vector as a function of d; (b) variation of the PK force as a function of d. In CSM, the Burgers vector of a single interface dislocation is equal to $0.05\boldsymbol{b}_s$. In SCSM, two different increments in the Burgers vectors are considered in the calculation: 0.025 and $0.001\boldsymbol{b}_s$. In SDSM, three different Burgers vectors are used: 0.30, 0.17 and $0.08\boldsymbol{b}_s$, where in all cases, $\boldsymbol{b}_s$ is the Burgers vector of the lattice dislocation.

model, agreement with the P–K force predicted by the CSM could be achieved by assigning the super dislocation a Burgers vector that is lower in magnitude from that of the net Burgers vector of the CSM.

4. Conclusions

In this paper, we propose three dislocation-based models for the onset and propagation of an interfacial shear region in response to an approaching lattice dislocation. The three models are called the continuous shear model (CSM), simple-CSM (SCSM) and single-dislocation-shear model (SDSM). In all three, interfacial shearing is accomplished by the nucleation of interfacial dislocations, which are modeled as a continuous distribution in the CSM, a super dislocation with a varying Burgers vector in the SCSM, and a super dislocation with a constant Burgers vector in the SDSM. In all calculations, the stress fields produced by the system of lattice and interfacial dislocations are calculated by means of a 2D Green's function method for two anisotropic crystals joined at a bi-material interface. We demonstrate that the models are all capable of predicting the interaction kinetics consistent with previous atomistic simulation. The CSM performs the best, effectively predicting the increase in interfacial dislocation content and extent of the sheared region as the interfacial dislocation draws closer to the interface. It also predicts the transition from a repulsive to attractive interaction caused by interfacial shearing and how the strength of this attraction is higher for interfaces weaker in shear. We show that with some optimization, SCSM and SDSM are able to reasonably capture the dislocation-interface interaction nearly as well as the CSM. The main advantage of SCSM and SDSM is that when implemented into higher length-scale models they can represent the essence of dislocation/interface interactions with significantly reduced computational burden.

While the present studies focused on the interaction between an incoming dislocation and an interface prior to impact, the results will be important for understanding what happens to the dislocation once it reaches the interface, where it must react with the interfacial dislocations. Details of this reaction will decide the fate of this dislocation, whether it is stored in the interface, reflected, transmitted, or re-emitted as a new lattice dislocation into the adjacent crystal, as discussed in Refs. (Wang and Misra, 2011; Hangen and Raabe, 1995; Raabe et al., 1995). The development of such models that describe slip transmission, dislocation reflection, and dislocation nucleation at interface is still an on-going goal. Currently we are working on the development of the model in describing slip transmission across interface, because atomistic simulations have systematically explored the physics of slip transmission with respect to interface structures and properties (Wang and Misra, 2011; Wang et al., 2012b; Wang et al. 2011b).

Acknowledgments

H.J. Chu, J. Wang and I.J. Beyerlein acknowledge support provided by a Los Alamos National Laboratory Directed Research and Development (LDRD) project DR20110029. J. Wang also acknowledges support provided by the US Department of Energy, Office of Science, Office of Basic Energy Sciences and a Los Alamos National Laboratory Directed Research and Development (LDRD) project ER20110573. Chu acknowledgements the financial support provided by the National Natural Science Foundation (10602050) and a Jiangsu Government Scholarship for overseas studies. Authors also thank Drs. N. Li, R.F. Zhang, C.Z. Zhou, K. Kang for their helpful discussions and suggestions in our regular group meetings.

References

Anderson, P.M., Li, Z., 2001. A Peierls analysis of the critical stress for transmission of a screw dislocation across a coherent, sliding interface. Materials Science and Engineering A 319–321, 182–187.
Akasheh, F., Zbib, H.M., Hirth, J.P., Hoagland, R.G., Misra, A., 2007. Dislocation dynamics analysis of dislocation intersections in nanoscale metallic multilayered composites. Journal of Applied Physics 101, 084314.
Ashmawi, W.M., Zikry, M.A., 2002. Prediction of grain-boundary interfacial mechanisms in polycrystalline materials. Journal of Engineering Materials and Technology 124, 88–96.
Balint, D.S., Deshpande, V.S., Needleman, A., Van der Giessen, E., 2008. Discrete dislocation plasticity analysis of the size dependence of the flow strength of polycrystals. International Journal of Plasticity 24, 2149–2172.
Barnett, D.M., Lothe, J., 1974. An image force theorem for dislocations in bicrystals. Journal of Physics F: Metal Physics 4, 1618–1635.
Barbe, F., Forest, S., Cailletaud, G., 2001. Intergranular and intragranular behavior of polycrystalline aggregates. Part 2: Results. International Journal of Plasticity 17, 537–563.
Bieler, T.R., Eisenlohr, P., Roters, F., Kumar, D., Mason, D.E., Crimp, M.A., Raabe, D., 2009. The role of heterogeneous deformation on damage nucleation at grain boundaries in single phase metals. International Journal of Plasticity 25, 1655–1683.
Beyerlein, I.J., Mara, N.A., Bhattacharyya, D., Necker, C.T., Alexander, D.J., 2011. Texture evolution via combined slip and deformation twinning in rolled silver–copper eutectic nanocomposite. International Journal of Plasticity 27, 121–146.
Brown, D.W., Beyerlein, I.J., Sisneros, T.A., Clausen, B., Tomé, C.N., 2012. Role of deformation twinning and slip during compressive deformation of beryllium as a function of strain rate. International Journal of Plasticity 29, 120–135.
Cao, F., Beyerlein, I.J., Addessio, F.L., Sencer, B.H., Trujillo, C.P., Cerreta, E.K., Gray III, G.T., 2010. Orientation dependence of shock induced twinning and substructures in a copper bicrystal. Acta Materialia 58, 549–559.
Chu, H.J., Pan, E., Wang, J., Beyerlein, I.J., 2011. Three-dimensional elastic displacements induced by a dislocation of polygonal shape in anisotropic elastic crystals. International Journal of Solids and Structures 48, 1164–1170.
Chu, H.J., Pan, E., Wang, J., Beyerlein, I.J., 2012a. Elastic displacement and stress fields induced by a dislocation of polygonal shape in an anisotropic elastic half-space. Journal of Applied Mechanics 79, 021011.
Chu, H.J., Pan, E., Han, X., Wang, J., Beyerlein, I.J., 2012b. Elastic fields of dislocation loops in three-dimensional anisotropic biomaterials. Journal of the Mechanics and Physics of Solids 60, 418–431.
Demkowicz, M.J., Wang, J., Hoagland, R.G., 2008. Interfaces between dissimilar crystalline solids. In: Hirth, J.P. (Ed.), Dislocations in Solids, vol. 14. Elsevier, Amsterdam, pp. 141–205.
Devincre, B., Hoc, T., Kubin, L., 2008. Dislocation mean free paths and strain hardening of crystals. Science 320, 1745–1748.
Erturk, I., Van Dommelen, J.A.W., Geers, M.G.D., 2009. Energetic dislocation interactions and thermodynamical aspects of strain gradient crystal plasticity theories. Journal of Mechanics Physics and Solids 57, 1801–1814.
Espinosa, H.D., Panico, M., Berbenni, S., Schwarz, K.W., 2006. Discrete dislocation dynamics simulations to interpret plasticity size and surface effects in freestanding FCC thin films. International Journal of Plasticity 22, 2091–2117.
Ghoniem, N.M., Sun, L.Z., 1999. Fast-sum method for the elastic field off three-dimensional dislocation ensembles. Physical Review B 60, 128–140.
Ghoniem, N.M., Tong, S.H., Sun, L.Z., 2000. Parametric dislocation dynamics: a thermodynamics based approach to investigations of mesoscopic plastic deformation. Physical Review B 61, 913–927.
Hangen, U., Raabe, D., 1995. Modelling of the yield strength of a heavily wire drawn Cu–20%Nb composite by use of a modified linear rule of mixtures. Acta Metallurgica 43, 4075–4082.
Hirth, J.P., Lothe, J., 1992. Theory of Dislocations. Krieger Publishing, Florida.
Hoagland, R.G., Hirth, J.P., Misra, A., 2006. On the role of weak interfaces in blocking slip in nanoscale layered composites. Philosophical Magazine 86, 3537–3558.
Hoagland, R.G., Mitchell, T.E., Hirth, J.P., Kung, H., 2002. On the strengthening effects of interfaces in multilayer fee metallic composites. Philosophical Magazine A 82 (A), 643–664.
Hu, S.Y., Li, Y.L., Zheng, Y.X., Chen, L.Q., 2004. Effect of solutes on dislocation motion – a phase-field simulation. International Journal of Plasticity 20, 403–425.
Hunter, A., Koslowski, M., 2008. Direct calculation of length scales in gradient plasticity. Journal of the Mechanics and Physics of Solids 56, 3181–3190.
Hunter, A., Beyerlein, I.J., Germann, T.C., Koslowski, M., 2011. Influence of the stacking fault energy surface on extended partials in fcc metals with a 3D phase field dislocation dynamics model. Physical Review B 84, 144108.
Koslowski, M., Cuitino, A., Ortiz, M., 2002. A phase–field theory of dislocations dynamics, strain hardening and hysteresis in ductile single crystals. Journal of the Mechanics and Physics of Solids 50, 2597–2635.
Liu, X.Y., Hoagland, R.G., Wang, J., Germann, T.C., Misra, A., 2010. The influence of dilute heats of mixing on the atomic structures, defect energetics and mechanical properties of fcc–bcc interfaces. Acta Materialia 58, 4549–4557.

Ma, A., Roters, F., Raabe, D., 2006. On the consideration of interactions between dislocations and grain boundaries in crystal plasticity finite element modeling – Theory, experiments, and simulations. Acta Materialia 54, 2181–2194.
Misra, A., Verdier, M., Lu, Y.C., Kung, H., Mitchell, T.E., 1998. Structure and mechanical properties of Cu-X (X = Nb, Cr, Ni) nanolayered composites. Scripta Materialia 39, 555–560.
Ohashi, T., 2005. Crystal plasticity analysis of dislocation emission from micro voids. International Journal of Plasticity 21, 2071–2088.
Pan, E., Amadei, B., 1999. Boundary element analysis of fracture mechanics in anisotropic bimaterials. Engineering Analysis with Boundary Elements 23, 683–691.
Raabe, D., Heringhaus, F., Hangen, U., Gottstein, G., 1995. Investigation of a Cu-20mass%Nb in situ Composite, Part I: fabrication, microstructure and mechanical, properties Part II: electromagnetic properties and application. Zeitschrift für Metallkunde 86, 405–422.
Roters, F., Eisenlohr, P., Hantcherli, L., Tjahjanto, D.D., Bieler, T.R., Raabe, D., 2010. Overview of constitutive laws, kinematics, homogenization, and multi-scale methods in crystal plasticity finite-element modeling: theory, experiments, applications. Acta Materialia 58, 1152–1211.
Shehadeh, M.A., Lu, G., Banerjee, S., Kioussis, N., Ghoniem, N., 2007. Dislocation transmission across the Cu/Ni interface. a hybrid atomistic–continuum study. Philosophical Magazine 87, 1513–1529.
Shen, C., Wang, Y., 2004. Phase field modeling of defects and deformation. Acta Materialia 52, 683–691.
Shen, Y., Anderson, P.M., 2006. Transmission of a screw dislocation across a coherent, slipping interface. Acta Materialia 54, 3941–3951.
Shen, Y., Anderson, P.M., 2007. Transmission of a screw dislocation across a coherent, nonslipping interface. Journal of the Mechanics and Physics of Solids 55, 956–979.
Smith, W.F., Hashemi, J., 2006. Foundations of Materials Science and Engineering, fourth ed. McGraw-Hill, New York.
Ting, T.C.T., 1996. Anisotropic Elasticity: Theory and Applications. Oxford University Press, New York.
Wang, C.Y., 1996. The stress field of a dislocation loop in an anisotropic solid. Journal of Mechanics and Physics of Solids 44, 293–305.
Wang, J., Hoagland, R.G., Hirth, J.P., Misra, A., 2008a. Atomistic simulations of the shear strength and sliding mechanisms of copper–niobium interfaces. Acta Materialia 56, 3109–3119.
Wang, J., Hoagland, R.G., Hirth, J.P., Misra, A., 2008b. Atomistic modeling of the interaction of glide dislocations with "weak" interfaces. Acta Materialia 56, 5685–5693.
Wang, J., Hirth, J.P., Pond, R.C., Howe, J.M., 2011a. Rotational partitioning at two-phase interfaces. Acta Materialia 59, 241–251.
Wang, J., Misra, A., Hirth, J.P., 2011b. Shear response of $\Sigma 3\{1\,1\,2\}$ twin boundaries in face-centered-cubic metals. Physics Review B 83, 064106.
Wang, J., Hoagland, R.G., Liu, X.Y., Misra, A., 2011c. The influence of interface shear strength on the glide dislocation–interface interactions. Acta Materialia 59, 3164–3173.
Wang, J., Misra, A., 2011. An overview of interface-dominated deformation mechanisms in metallic multilayers. Current Opinion in Solid State and Materials Science 15, 20–28.
Wang, J., Beyerlein, I.J., 2012. Atomic structures of symmetric tilt grain boundaries in hexagonal close packed (hcp) crystals. Modelling and Simulation in Materials Science and Engineering 20 (2), 024002.
Wang, J., Beyerlein, I.J., Hirth, J.P., 2012a. Nucleation of elementary $-1\,0\,1\,1$ and $-1\,0\,1\,3$ twinning dislocations at a twin boundary in hexagonal close-packed crystals. Modelling and Simulation in Materials Science and Engineering 20 (2), 024001.
Wang, J., Misra, A., Hoagland, R.G., Hirth, J.P., 2012b. Slip transmission across fcc/bcc interfaces with varying interface shear strengths. Acta Materialia 60, 1503–1513.
Wang, Z.Q., Ghoniem, N.M., 2006. A parallel algorithm for 3D dislocation dynamics. Journal of Computational Physics 219, 608–621.
Zbib, H.M., Overman, C.T., Akasheh, F., Bahr, D., 2011. Analysis of plastic deformation in nanoscale metallic multilayers with coherent and incoherent interfaces. International Journal of Plasticity 27, 1618–1639.